Electronic Structure of Palladium

F. M. Mueller*
Argonne National Laboratory, Argonne, Illinois 60439
and
A. J. Freeman†
Physics Department, Northwestern University, Evanston, Illinois 60201
and Francis Bitter National Magnet Laboratory,‡ Massachusetts Institute of Technology, Cambridge, Massachusetts 02139
and
J. O. Dimmock
Lincoln Laboratories,§ Massachusetts Institute of Technology, Lexington, Massachusetts 02173
and
A. M. Furdyna
Francis Bitter National Magnet Laboratory‡ Massachusetts Institute of Technology, Cambridge, Massachusetts 02139
(Received 26 September 1969)

A detailed investigation of the electronic structure of palladium is presented in terms of two different band models: (1) *ab initio* calculations using the augmented-plane-wave method, and (2) calculations using the combined interpolation scheme augmented by inclusion of relativistic corrections. The width and position of the *d*-band complex are found to be particularly sensitive features of the electronic structure of palladium. A highly detailed density-of-states histogram, and estimates for the first and second derivatives of the density of states at the Fermi energy are derived. In addition, detailed comparisons are made with Fermi-surface–static susceptibility, and specific-heat experimental results. Estimates for the effects of many-body enhancements suggest that paramagnons raise the effective mass at the Fermi energy by only about 41%. Owing to the strong *s-d* hybridization in palladium, the Fermi surface is made up almost entirely of *d*-like states. Because the Fermi energy in palladium falls near the strongly spin-orbit split levels at *X* and *L*, spin quenching reduces the effective *g* factor at the Fermi energy from 2 to about 1.65. This increases an estimate of the effective Stoner-enhancement factor from 10 to about 15.

I. INTRODUCTION

Even among transition metals, palladium is outstanding because of its unusual properties. It has a very high magnetic susceptibility which shows an anomalous temperature dependence[1] at low temperatures, and it has one of the highest electronic specific heats[2] for metals. Recently, considerable interest has been aroused by the observation of localized moments on very dilute impurities alloyed with palladium, and by the occurrence of ferromagnetism in the dilute alloys of 3*d* and 4*d* transition metals[3] with palladium. Indeed, this tendency toward strong magnetic behavior, expressed in its being an "incipient ferromagnet," makes the study of palladium so interesting. Particularly important has been the microscopic nature of the exchange enhancement of the susceptibility[4] and the role of this enhancement in the theory of spin fluctuations.[5] Little was known quantitatively about either the band structure or the Fermi surface of palladium until recent galvanomagnetic,[6] and de Haas–van Alphen[7] experiments gave precise information about a number of features of the Fermi surface. Prior to our preliminary report,[8] little theoretical information was available for comparison with experiment or for understanding the origin of the magnetic properties of palladium. Since the conduction electrons of palladium are isoelectronic to those of nickel, which is ferromagnetic, a theoretical study of palladium is particularly desirable.

The results presented here include the complete band structure of metallic palladium, as determined by means of nonrelativistic augmented-plane-wave[9] (APW) calculations, and the density of states, the magnetic susceptibility, and Fermi surface obtained from these *ab initio* calculations. The Fermi surface, which consists of two hole surfaces and a compensating electron surface, agrees well with the de Haas–van Alphen data of Vuillemin and Priestly.[7] The electron surface is centered at the point Γ and contains approximately 0.36 electrons per palladium atom. One hole surface consists of a small pocket centered at *X*. The other hole surface is in the form of a series of cubic-arranged interconnecting pipes which are open along the $\langle 100 \rangle$ directions in agreement with galvanomagnetic measurements.[6] The Fermi energy lies slightly above the maximum in the calcu-

lated density of states $N(E)$, which occurs at the top end of the d-band region of fcc transition metals. This result was expected from studies of palladium alloyed with the neighboring elements rhodium and silver.[1,10] The computed $N(E_F)$ yielded an electronic contribution to the specific heat which is only about half the observed value, indicating a total many-body enhancement typical for d-band metals. The computed paramagnetic susceptibility $\chi(T)$ is much smaller than the experimental value; this emphasizes the importance of exchange in markedly enhancing $\chi(T)$, particularly at low temperatures.

Our theoretical band structure was brought into even closer agreement with experimental data by use of the combined interpolation scheme,[11] which allows us to add a spin-orbit coupling adjustment of the nonrelativistic energy bands. The interpolation scheme, originally designed to treat $3d$ metals, was modified to accommodate the increased relativistic effects and wider d-band complexes exhibited by the $4d$ metals. The modified interpolation scheme was used to derive interpolation bands which are in good agreement with all three initial APW band calculations.

The atomic configuration $4d^{10}5s^0$ was used to simulate the self-consistent palladium potential. If the observed[7] number of electrons in palladium, 0.36, is entirely s-like, the appropriate muffin-tin potential would arise from the atomic configuration $4d^{9.6}5s^{0.4}$. The simulation is therefore reasonable. Moreover, full Hartree-Fock-Slater exchange was used. Previous use of this exchange in other metals yielded good agreement with both Fermi-surface experiments and optical properties. In the present work, the amount of spin-orbit coupling was adjusted so as to reproduce a few critical Fermi-surface areas.

Based on the adjusted relativistic band structure, calculations were made of the Fermi-surface radii and an accurate electronic density of states. From the density of states and Stoner-Wohlfarth[12] formulas, the temperature and magnetic field dependence of the paramagnetic susceptibility χ were calculated.

All of the earlier results of the *ab initio* APW calculations are in qualitative agreement with those produced by the interpolation scheme. By combining both *ab initio* and interpolative methods results are obtained which can be confidently compared with experiment.

II. *AB INITIO*

The electronic energy bands of palladium were derived using the nonrelativistic APW method of Slater[9] and three different approximate crystal potentials. The crystal structure of palladium is fcc and the lattice parameter used is $a = 7.353$ a.u. The potentials were formed from a superposition of spherically symmetrical atomic potentials generated from free-atom Hartree-Fock-Slater wave functions[13] for the atomic configurations $4d^{10}5s^0$

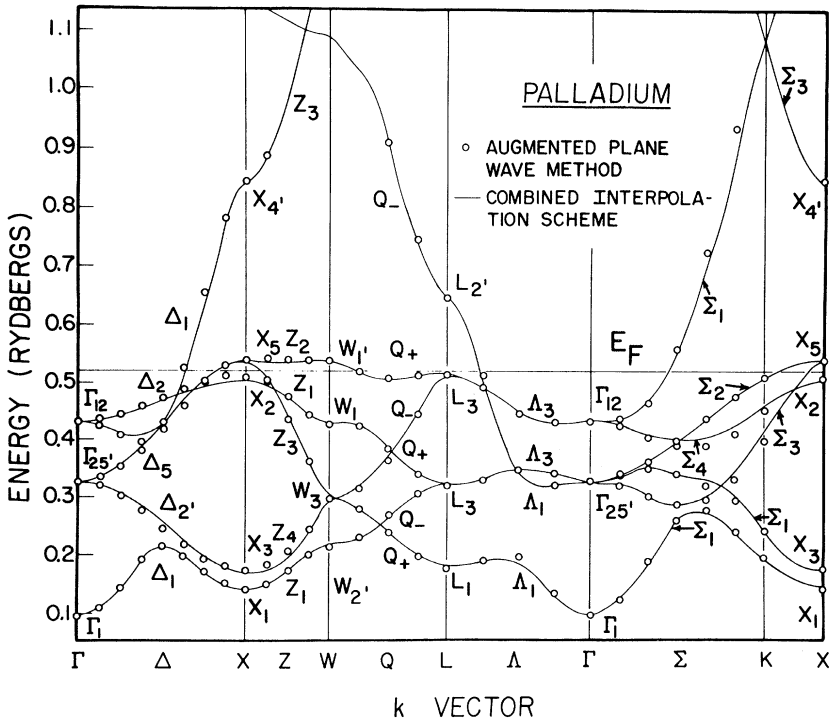

FIG. 1. Electronic band structure of palladium. Open circles are nonrelativistic APW energy levels produced from a potential formed from atomic wave functions of configuration $4d^{10}5s^0$ and full HFS exchange. Solid lines are energy bands produced by the combined interpolation scheme using the parameters of Table III, case 2. Close agreement between the results suggests that the accuracy of the interpolation fit is high.

and $4d^9 5s^1$. Analytic atomic Hartree-Fock functions[14] were also used for the configuration $4d^{10}5s^0$. In the first two calculations, the effects of exchange were approximated by using the full value of the Slater $\rho^{1/3}$ free-electron exchange. In the last calculation, the exchange is of the Hartree-Fock form and was included in the superimposed atomic potentials.

Most of the results presented here are based on the energy bands shown in Fig. 1 and obtained from the Hartree-Fock-Slater $4d^{10}5s^0$ potential. The d bands calculated for palladium are somewhat broader than those usually found for copper, silver, or nickel. Some results of the Hartree-Fock-Slater (HFS) and Hartree-Fock (HF) calculations are shown in Table I. The upward motion of the d bands with respect to the s-p bands increases with d content in the potential. Conversely, the exact form of the potential has little effect on the relative positions of the s-p band states X_4' and L_2'. In the analytic HF $4d^{10}5s^0$ calculation, the d band is about 14% broader and approximately 0.1 Ry higher with respect to the s-p band than in the HFS $4d^{10}$ calculation. Although this latter calculation gives a very good representation of the experimental data on palladium, these differences suggest uncertainties in the potential. These calculations will be compared and discussed in more detail in Sec. III.

Energy eigenvalues were calculated at 89 inequivalent points in the $\frac{1}{48}$ wedge of the Brillouin zone for the HFS $4d^{10}$ potential. From these eigenvalues, a crude density of states $N(E)$ was constructed for the d and conduction electron bands by dividing the Brillouin zone into identical polygons, each characterized by the energy calculated at its center. From the $N(E)$ curve the position of the Fermi energy was found to be that energy at which ten electrons per atom are accommodated. The crude histogram representation is shown in Fig. 2. The value of the density of states at the Fermi energy, $N(E_F)$, was found to be 28.2 states/atom Ry. This value is in reasonable agreement with that in the valence-band optical density of states of palladium deduced from photoemission and reflectivity data obtained by Yu and Spicer[15] and Eastman.[16] A more accurate $N(E)$ curve is presented later, as well as extensive comparisons with magnetic susceptibility, electronic specific heat, and other data. Figure 2 is presented here for historical interest; it has been used in other workers' publications and will be compared with the predictions presented later in our discussion of the combined interpolation scheme.

TABLE I. Comparison of the calculated eigenvalues for palladium (Ry).

	$(4d)^9(5s)^1$	$(4d)^{10}(5s)^0$	$(4d)^{10}$ Anal.
Γ_1	0.000	0.000	0.000
Γ_{25}'	0.180	0.232	0.326
Γ_{12}	0.277	0.335	0.441
X_1	0.011	0.047	0.109
X_3	0.036	0.078	0.154
X_2	0.352	0.414	0.528
X_5	0.379	0.443	0.559
X_4'	0.749	0.751	0.753
L_1	0.047	0.082	0.143
L_3	0.173	0.224	0.316
L_3	0.356	0.418	0.532
L_2'	0.550	0.551	0.552
X_5-X_1	0.368	0.396	0.450

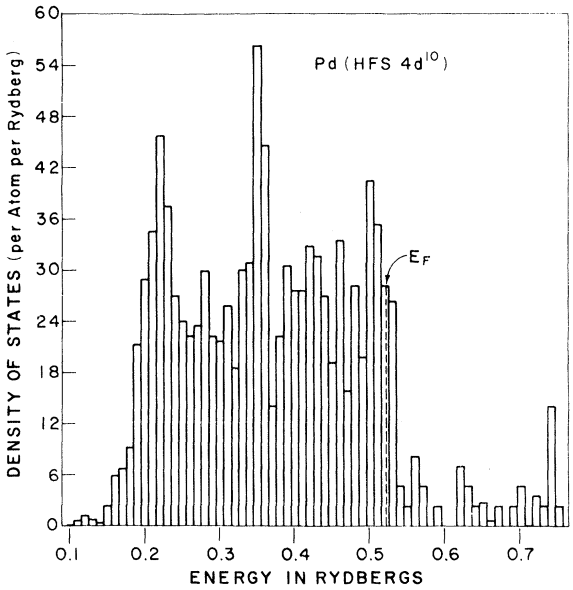

FIG. 2. Density of states of palladium as calculated directly from 89 unequivalent points produced by means of the APW method for the $4d^{10}5s^0$ (HFS) potential. Value of the density of states at the Fermi level obtained from the calculation is presented in Fig. 6, where a larger number of sampling points were used.

The Fermi surface of palladium was calculated from the energy bands shown in Fig. 1. Figures 3 and 4 show the approximate electron and open-hole sections of the Fermi surface. As can be seen from Fig. 1, the calculation also yields small ellipsoidal pockets of holes centered at X. The total volume of the holes is approximately 10^{-2} holes/atom. In many ways, the most interesting section of the Fermi surface is the open (heavy) hole surface shown in Fig. 4. This "jungle-gym" structure is evident in the expanded zone representation used in the figure.

The Fermi surface of palladium was first studied by Vuillemin and Priestley,[7] who found an electron surface which was centered about the point Γ and which contained 0.36 ± 0.01 electrons/

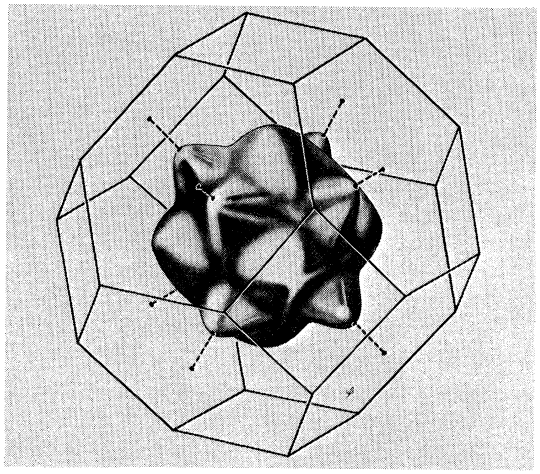

FERMI ELECTRON SURFACE FOR PALLADIUM

FIG. 3. Γ-centered sixth-band electron sheet of palladium. Although topologically equivalent to a sphere, this sector of the Fermi surface shows large distortions. As is discussed in the text, the sheet is primarily *d* like rather than plane-wave-like.

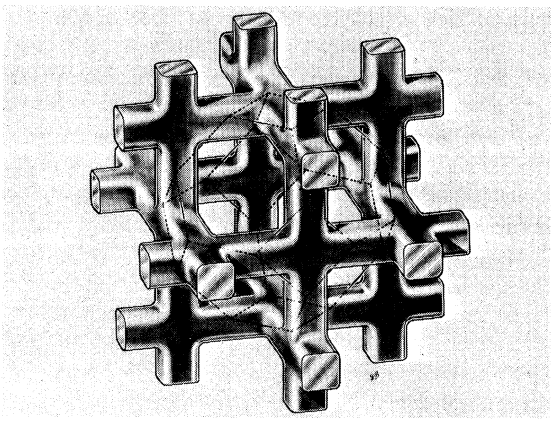

FERMI HOLE SURFACE FOR PALLADIUM

FIG. 4. *X*-centered hole sheet of palladium. This sheet is formed from the fifth-band electrons and forms an open network in the extended zone. As is discussed in the text, this sheet is primarily *d*-like.

atom. They also found small pockets of holes which were centered at the *X* points and which contained a total of 5.4×10^{-3} holes/atom. Since palladium is a compensated metal, approximately 0.36 holes/atom are unaccounted for in these results. On the other hand, galvanomagnetic data of Alekseevskii, Karstens, and Moshaev[6] show that part of the Fermi surface of palladium is open and topologically equivalent to a spatial network of cylinders with axes directed along the ⟨100⟩ directions. This part would then contain the missing holes. Recently, this sheet of the surface has been seen by means of the de Haas–van Alphen (dHvA) effect.[17]

Agreement is surprisingly good between the experimental Fermi-surface data and the computed electron and open-hole sections of the Fermi surface. The experimental shapes and volumes are all reasonably well reproduced by the calculations. For example, the Γ-centered electron surface contains approximately 0.3 electrons/atom and displays the same sort of humps as found experimentally. The experimental value of 0.36 electrons/atom is certainly well within the uncertainties of the *ab initio* calculation. The open-hole surface shown schematically in Fig. 4 contains approximately 0.3 holes/atom as required for compensation. In order to increase the electron volume to 0.36 electrons/atom, it would be necessary to lower the *s-p* band with respect to the *d* band by about 0.05 Ry, an operation which is within the uncertainties of the calculation. This adjustment would increase the total volume of the small-hole pockets by about 30%. Since in the nonrelativistic calculation, the light-hole band is pinned to the heavy-hole band at the *X* point and along the line Γ-*X*, the volume of the small-hole pockets cannot change very much without an accompanying change in the electron and heavy-hole volumes. As is discussed below, this constraint is removed when relativistic effects are considered.

The importance of relativistic effects for the near-noble metals can be estimated from Table II which shows the relativistic effects for the valence electrons in atomic nickel, palladium, and platinum, calculated by Herman and Skillman[13] from nonrelativistic HFS wave functions. The approximate shift of the *d* and *s-p* bands are given by ΔE_d (shift) and ΔE_s (shift), respectively. In each case, the difference between these values is very small, and relativistic effects would not greatly change the relative positions of the *d* and *s-p* bands. The most prominent effects on the band structure are the lifting of degeneracies by spin-orbit splitting

TABLE II. Relativistic effects of the valence electrons of Ni, Pd, and Pt (Ry) (after Herman and Skillman, Ref. 13).

	$Ni(3d)^8(4s)^2$	$Pd(4d)^{10}(5s)^0$	$Pt(5d)^9(6s)^1$
ΔE_d(shift)	−0.0165	−0.0370	−0.1328
$\Delta E_d(s\text{-}o)$	0.0204	0.0370	0.1148
ΔE_s(shift)	−0.0180	−0.0362[a]	−0.1282
$(\Delta E_s-\Delta E_d)$ (shift)	−0.0015	0.0008	0.0046

[a]Estimated.

and the related prevention of the crossing of bands along certain symmetry lines. Both effects can, in some cases, have a marked influence on the Fermi-surface topology, as discussed below. In the cases of palladium and of platinum, the most important effect is the relativistic spin-orbit splitting of energy bands in the vicinity of the X and L points.

Recently, Andersen and Mackintosh[18] calculated the energy band structure of rhodium, palladium, iridium, and platinum using the relativistic APW method of Loucks.[19] These calculations concentrated on the energy bands in the vicinity of the Fermi energy and were concerned with obtaining accurate Fermi-surface cross sections and effective masses as well as the density of states at the Fermi energy. More recently, Freeman and Koelling[20] studied the energy bands for several different atomic configurations of platinum over a wide energy range. They used the symmetrized relativistic APW method and a variable Slater free-electron exchange approximation. In both calculations, relativistic effects were important in determining the energy band structure, especially of the heavy metals, iridium and platinum. For example, if the results obtained for platinum were scaled down by the ratio of the atomic spin-orbit splittings in palladium and platinum, 0.322, a splitting of about 0.026 Ry would occur at the X point in palladium. As can be seen from Fig. 1, the splitting would have a dramatic effect on the small-hole pockets. Relativistic effects are important in determining such details, although they may not alter the gross features of the band structure. For example, comparison of the relativistic and nonrelativistic energy bands in platinum along the Γ-X direction clearly shows the effects of spin-orbit splitting with little difference in the relative positions of the d and s-p bands.[18,20]

The *ab initio* APW method, by itself, includes a number of uncertainties in calculating energy bands and Fermi surfaces in transition metals. Since the conduction bands in the transition metals are composed of hybridized d and s-p bands, the relative positions of these bands are important in determining the major features of the energy band structure. Furthermore, due largely to the different spatial extent of the d and s-p functions, these relative positions are the most sensitive to the crystal potential. In the present calculations (Table I), a difference of approximately 0.06 Ry was found in the relative positions of the d and s-p bands in palladium depending on whether a $4d^9 5s^1$ or $4d^{10} 5d^0$ atomic configuration was used in calculating the crystal potential for palladium. Also, Snow, Waber, and Switendick[21] found about a 0.1-Ry shift between the relative positions of the d and s-p bands in nickel depending on whether they used a $3d^9 4s^1$ or $3d^{10} 4s^0$ atomic configuration in calculating the crystal potential. Our smaller shifts may be due to a smaller difference between the spatial extent of the $4d$- and $5s$-p wave functions in palladium. With uncertainties of this magnitude only the gross aspects of the band structure can be obtained.

In addition, since these large variations depend on the assumed atomic configurations, the calculations should be performed self-consistently. However, even with self-consistency, the somewhat arbitrary choice of the exchange potential has a large effect, especially on the relative positions of the d and s-p bands. Snow[22] has performed self-consistent APW calculations on copper and silver using both the full value of the Slater free-electron exchange approximation and $\frac{5}{6}$ of this value. In these calculations, the d bands are found to lie about 0.1 Ry higher with respect to the s-p bands in the $\frac{5}{6}$ exchange calculation than in the full exchange calculation. Consequently, owing to uncertainties in the exchange potential (~ 0.1 Ry), large uncertainties exist even in calculations performed self-consistently.

Unless a more accurate method is developed for calculating the effective independent-particle exchange energy, including correlation effects, the determination of highly accurate energy bands of transition metals requires an adjustment of the energy bands to fit experiment. The Fermi surface of the noble metals is less sensitive to the potential, since the Fermi energy lies in a region of s-p-like energy bands. In transition metals, the Fermi energy lies in the midst of the d bands, and the Fermi surface is highly sensitive to the relative positions of the energy bands. In extreme cases, even the gross features of the Fermi surface must be determined almost entirely by experiment. Nevertheless, the general features of the energy bands themselves can in most cases be determined by the *ab initio* calculations.

III. COMBINED INTERPOLATION SCHEME

In this section and in Appendix A, the application of the combined interpolation scheme to the calculation of the band structure of palladium is discussed. First considered are the modifications which make the scheme able to treat $4d$ transition metals. A discussion of the methods used to find parameters for the scheme from APW results is presented in Appendix B. Using these parameters, several comparisons are then made between the bands found from the three different potentials. Finally, the APW results are augmented by adding relativistic effects within the interpolation scheme

and three ways of deriving relativistic parameters for the scheme are considered.

A. Modifications of the Combined Interpolation Scheme

Unlike the APW method, which finds the band structure $E_n(k)$ of palladium through a direct solution of Schrödinger's equation with a given form of potential, the combined interpolation scheme adopts a method which is indirect and finds the bands as a function of certain parameters which may be interpreted as various overlap or transfer integrals of given basis functions. In the free atom, palladium has three configurations, $4d^85s^2$, $4d^95s^1$, and $4d^{10}5s^0$; all have roughly the same energy eigenvalues. Band structures calculated by the APW method all exhibit narrow bands of d character crossed by broad bands of mixed $5s$-$5p$ or nearly free-electron character. Examination of Fig. 1, which contains both the initial APW results and the final combined interpolation scheme fit, shows that the basic assumption of the combined interpolation scheme is well justified. A mixed basis set of d electrons as either tight-binding or Wannier functions[23] and of plane waves orthogonalized to both d and core states well approximates the physical structure of the eigenfunctions of the Hamiltonian. An exact representation of crystallographic group symmetries is preserved within the truncated basis set.

The case of palladium differs from the previously treated case of copper[11] in two ways: First, in palladium, d states occur in both the core and the conduction bands; second, relativistic effects are much stronger in palladium than they are in copper. The additional core d states require extension of the combined interpolation scheme by orthogonalizing the plane-wave states $|\varphi_k\rangle$ to not only the d conduction-band states but also to the core $3d$ states.

If the $3d$ band of palladium is sufficiently narrow, an effective core d local pseudopotential can be formulated and the $3d$ orthogonality terms cause negligible corrections to the energy bands produced by the original interpolation scheme. Thus, the combined interpolation scheme can be adopted without structural change, and the results can be interpreted in terms of $4d$ basis states. Five d basis functions are used of angular symmetry xy, xy, yz, $\frac{1}{2}(x^2-y^2)$, and $(4\sqrt{3})^{-1/2}(2z^2-x^2-y^2)$ times a common radial function $f(r)$. The minimum number of plane-wave basis states which can accurately simulate the palladium bands are used in order to have the smallest possible secular equation. For a fcc lattice those are the lowest four plane waves degenerate at the point W in the Brillouin zone.

The restricted Hamiltonian made up from these two types of basis states yields a 9×9 secular matrix and contains terms of three different types. These are written as $\langle d|H|d\rangle$, $\langle d|H|\varphi\rangle$, and $\langle\varphi|H|\varphi\rangle$, where $|d\rangle$ is any part of the five d states, and $|\varphi\rangle$ is any of the four orthogonalized plane-wave states. The matrix elements of two blocks $\langle d|H|\varphi\rangle$ and $\langle\varphi|H|\varphi\rangle$ are given in terms of two pseudopotential terms V_{111} and V_{200} (which correspond to the uncancelled effects of s, p, and d core states at two Bragg planes), the orthogonality parameters A and LR_0 [which correspond to $4d$ (bare) plane-wave overlap $\langle d|\vec{k}\rangle$, where $|\vec{k}\rangle$ is a plane wave], and the hybridization parameters B and LR_1 (which correspond to the mixing of conduction-band-d and orthogonalized-plane-wave states by the Hamiltonian). Note that although $\langle d|\varphi\rangle\equiv0$, this is not sufficient to guarantee that $\langle d|H|\varphi\rangle=0$. The hybridization parameters simulate this difference in the interpolation scheme. The matrix elements of the block $\langle d|H|d\rangle$ were previously given[11] in terms of a one-centered overlap integral d_0, the position of the d-band complex relative to the energy of the lowest plane-wave state at the point[24] $\Gamma(\equiv\Gamma_1)$; of three two-centered overlap integrals $dd\sigma$, $dd\pi$, and $dd\delta$; and of γ, the effective splitting of symmetry states of type xy and $\frac{1}{2}(x^2-y^2)$. This parametrization of the $\langle d|H|d\rangle$ block was based on the two-centered approximation, which has an accuracy of about 8% in both copper and palladium. The extension of the sums in $\langle d|H|d\rangle$ to full three-centered terms changes an average band energy by about 8% of the half d-band width, or by about $(0.08)\frac{1}{2}(0.2)$ Ry $=0.008$ Ry. This accuracy was sufficient for calculating the density of states of copper to only 5% vertical accuracy. However, 1% vertical accuracy was desired for palladium. Moreover, the $4d$ band in palladium is twice as wide as the $3d$ band in copper. Use of the two-centered approximation would therefore result in a large error $(0.08)\frac{1}{2}(0.4)$ Ry $=0.016$ Ry. Examination of Table V of Ref. 11 shows that modification of the parametrization scheme to include two $dd\pi$'s (one for the sum of P_4 and P_5, and one for P_8) would leave a residual error of about 2%, or 0.004 Ry, for palladium.

Since palladium is a heavy metal ($Z=46$), relativistic corrections must be included in order to compare theoretical results with experiment. The largest relativistic correction to the model Hamiltonian given above is spin-orbit coupling. The effective potential caused by spin-orbit coupling is given by

$$H_{so}=\sum_{R_m}-\tfrac{1}{2}\lambda(|\vec{r}-\vec{R}_m|)(\vec{\sigma}\cdot\vec{L}), \qquad (1)$$

where the sum is taken over all lattice sites

$\vec{R}_m$, where $\lambda(r) \equiv (e\hbar/4m^2c^2)(1/r)(\partial V/\partial r)$, (V/r) is the potential, and $\vec{L}$ begins on every lattice site.

Each of the blocks of the model Hamiltonian is affected by the correction given by Eq. (1). However, a number of simplifying approximations allow easy treatment of terms represented by Eq. (1). The first occurs in the d-d block. Since second-neighbor overlap integrals are <0.001 Ry, a good treatment of the copper d bands could be given in terms of the first-neighbor overlap integrals (~0.022 Ry) alone. In this case, $dd\sigma(1) \cong 20 \times dd\sigma(2)$, etc., where (1) and (2) are neighbor terms. This ratio suggests that, in the fcc lattice, the relation $\psi(R_1) \sim 20\psi(R_2)$ holds for d bands, where ψ is now an average d radial wave function at first- and second-neighbor distances, respectively. As in the full Hamiltonian, the terms introduced by Eq. (1) have zeroth-, first-, and second-neighbor terms connected by a structure factor. The effective range of Eq. (1) is so short and the radial part of the $4d$-state wave function drops off so quickly that, not only second-neighbor terms of Eq. (1), but also first-neighbor terms are unimportant. Thus, in the d-d block the problem reduces to a wholly atomic (i.e., single-center) problem. This approximation was also used for d-d block spin-orbit coupling by Friedel, Lengart, and Leman,[25] by Hodges, Ehrenreich, and Lang,[26] and by Mattheiss.[25] In Appendix A, it is shown that the spin-orbit coupling corrections to the d-OPW and OPW-OPW blocks are small using estimates of the band radial d-wave function and the effective potential by atomic[27] values. The derivation is similar to that given by Weisz[28] and shows that their angular dependence is given by cross- and dot-product terms of $\vec{k}$ and $\vec{k}'$. These terms have therefore been neglected in the calculations.

B. Discussion of Results of Fits

Three sets of palladium parameters were found for the modified combined interpolation scheme using the fitting techniques just discussed. This section examines these parameters. At this point, d-d spin-orbit coupling is neglected.

The three APW band structures examined above were found from potentials derived from various initial atomic configurations and different approximations to the effects of electronic exchange. Our sets of parameters were derived from the band structures using in each case exactly the same form of the Hamiltonian and fitting procedure. These three sets of parameters contain the similarities and differences of the three band structures and potentials in an extremely compact and accessible form. Thus, the interpolation scheme, in addition to fulfilling its role as a fitting procedure of *ab initio* band structures, also has uses as a tool for detailed analysis.

Table III lists the sets of parameters for the interpolation scheme which correspond to the three different palladium potentials. In each case, the zero of the energy scale has been reset so that the lowest plane-wave level Γ_1 corresponds exactly to zero. The average position of the d-band complex with respect to the plane-wave bands is given by the parameter d_0 which is measured relative to Γ_1. The variation of this parameter between the three cases shows the sensitivity of the posi-

TABLE III. Values of parameters for combined interpolation scheme for APW calculations of palladium.

	Parameters		1 $4d^95s^1$(HFS)	2 $4d^{10}5s^0$(HFS)	3 $4d^{10}5s^0$(HF)
d bands	p_i	v_i			
	d_0[a]	0.0100	0.2458	0.3064	0.3920
	$dd\sigma$	0.0010	−0.0427	−0.0447	−0.0497
	$dd\pi_1$	0.0010	0.0143	0.0138	0.0182
	$dd\pi_2$	0.0010	0.0153	0.0158	0.0192
	$dd\delta$	0.0001	−0.0007	−0.0002	−0.0016
	γ	0.0005	+0.0026	−0.0002	+0.0052
Conduction bands	V_{111}[b]	0.0010	0.0100	0.0100	0.0100
	V_{200}	0.0010	0.0033	0.0023	0.0093
Orthogonality	A	0.0500	1.3752	1.4813	1.6095
	LR_0	0.0050	2.0841	1.8403	2.1625
Hybridization	B	0.0500	1.4534	1.5041	1.5447
	LR_1	0.0050	2.6782	2.5979	2.6403
Spin orbit	E_p	0.0010	•••	0.0107	•••
Fermi energy	E_F[a]	0.0010	•••	0.4224	•••
Deviation of fit	$D(\vec{p})$	•••	0.0057	0.0048	0.0074

[a]Given relative to $\Gamma_1 = 0$ in each case.

[b]Not varied in fits.

tion of the d bands to the detailed shape of the potential. Such sensitivity has been emphasized by other workers.

The difference between the position of the d bands for the two configurations $4d^9 5s^1$ (case 1) and $4d^{10}5s^0$ (case 2), both calculated in HFS approximation, is due to the average net electron charge configuration being a little more extended out toward the Wigner-Seitz radius in the first case than the second. The potential appears a little stronger at short radius in the first case than the second. The orthogonalized plane-wave bands also shift their net position between the two configurations, relative to the vacuum level. However, the plane-wave shift is at least an order of magnitude smaller than the d shift. Consider that plane-wave state associated with Γ_1. The energy position of this level may be found from the net average of the potential of the unit cell. Since the actual change in the charge density between the two cases is negligible, and since the potential average is dominated by regions away from the ion core, the plane-wave bands are fixed and insensitive to the small-charge shifts corresponding to different atomic configurations. The d-radial wave functions peak in a region where the shift in effective charge density between the two configurations is maximum. Thus, the sensitivity of the position of the levels to such charge shifts is amplified.

Table III also compares the two d_0 parameters obtained from the APW band calculations derived from potentials found from a $4d^{10}5s^0$ atomic configuration either in HFS approximation (case 2) or in HF approximation (case 3). As in the atomic case, the effect of adding full Slater exchange to the Hamiltonian is to lower the d states relative to s-p states. The potential used in the APW calculations might have been derived using a configuration of $4d^{10}5s^0$, but from other than full Slater exchange.[29] For example, $\frac{2}{3}\rho^{1/3}$, i.e., the Kohn-Sham value of exchange,[30] might have been used. The primary effect on the electronic band structure would have been to make d_0 intermediate between case 2 and case 3, and to roughly scale d_0 proportionately by the amount of full Slater exchange between the limiting values given in Table III.

The d-d overlap parameters, $dd\sigma$, $dd\pi_1$, and $dd\pi_2$ are also given in Table III. The d-band width of these parameters in case 2 is only about 5% greater than in case 1, whereas case 3 is about 20% greater than case 1. This behavior is consistent with the virtual-resonance ideas of Heine.[31]

A similar situation occurs in the ratios of the orthogonality and hybridization amplitude parameters A and B determined for the different cases. These ratios are 1.09 and 1.04 between cases 2 and 1, and 1.17 and 1.06 between cases 3 and 1. According to Heine's theory, these ratios should scale as $W^{1/2}$ and W, respectively, where $W = E_F - E_d$. Although our ratios do not agree exactly with Heine's theory, these parameters again follow the qualitative behavior of the resonance ideas.

The radial strength parameters R_0 and R_1 represent a trading off between compacting the radial d-wave function to more effectively screen the nuclear charge, and the additional exchange energy which such compacting produces. The effective radius of peak interaction, R_1, remains roughly constant, whereas R_0 seems to have no consistent behavior. Perhaps no simple physical insight can be derived from these two rather complicated parameters. They may merely be regarded as adjuncts of the interpolation scheme. In a similar vein are the parameters $dd\delta$, γ, V_{111}, and V_{200}. However, even these "unphysical" parameters help to reduce fitting errors. Although a simple interpretation cannot be immediately attached to these parameters, they are not necessarily useless. Indeed, if all of these last four parameters were set equal to zero, the net fitting error for case 2 would increase by 0.003 Ry (= 0.008 – 0.005).

C. Addition of Spin-Orbit Coupling

The three sets of parameters for the scheme are almost sufficient to give results comparable with experiment. However, the parameters do not include relativistic effects. Although relativistic effects in palladium are not nearly as large as they are in platinum,[17,19,32] the lifting of various degeneracies make them important in the net palladium band structure and in determining Fermi-surface dimensions.

Relativistic corrections to the Schrödinger equation involve three terms. Two of these, the Darwin and the mass-velocity terms, yield only small corrections. A direct consideration of these two terms for platinum[32] showed that residual corrections were small and could be simulated by changing the free-electron mass by 5%. In palladium these effects are probably smaller by a factor of 3.

The third term, which is not small in palladium, is the spin-orbit coupling term. As discussed above, such effects are included in the interpolation scheme only through an atomiclike interaction acting on the d electrons alone. The net relativistic correction term H_{so}, added to the Hamiltonian, is then

$$H_{so} = \tfrac{1}{2} E_p \vec{\sigma} \cdot \vec{L}, \qquad (2)$$

where E_p is a parameter to be discussed below,

$\vec{\sigma}$ are the Pauli spin matrices, and $\vec{L}$ is the angular momentum operator here acting on d states alone.

Three different methods have been used to derive values for the parameter E_p in palladium. First, E_p was found by examining free-atom term values and assuming that the value of $4d$ spin-orbit coupling in the atom and the solid is the same. This procedure gave the value 0.026 Ry which was also the value used earlier.[25,26] In the absence of other information such extractions from the atom are often helpful in establishing trends over several different materials. However, wave functions do change between the atom and the solid and the changes are often particularly large for d states in transition metals.

The second method was to rescale the value of the doublet splitting in the calculation of Andersen and Mackintosh[18] for palladium by the ratio of the experimentally derived splitting for platinum to their theoretical splitting.[18] This method gave a value of 0.023 Ry for the parameter.

The last method used the experimental dHvA data. The size of the δ orbit[17] centered at W is very sensitive to the value of the spin-orbit coupling parameter. Therefore, the parameter E_p was varied in conjunction with those parameters derived from the $4d^{10}5s^0$ (HFS) configuration until this orbit's area was fit. This $4d^{10}5s^0$ configuration best represents the potential found from a truly self-consistent procedure. By this method a value of 0.021 was obtained for E_p. The variation between the values of E_p produced by the three methods suggest that this parameter is very sensitive and that caution should be exercised in the technique used to derive its value 0.021 produced by the dHvA data[16] as well as the parameters found from fitting the APW results using the $4d^{10}5s^0$ (HFS) configuration.

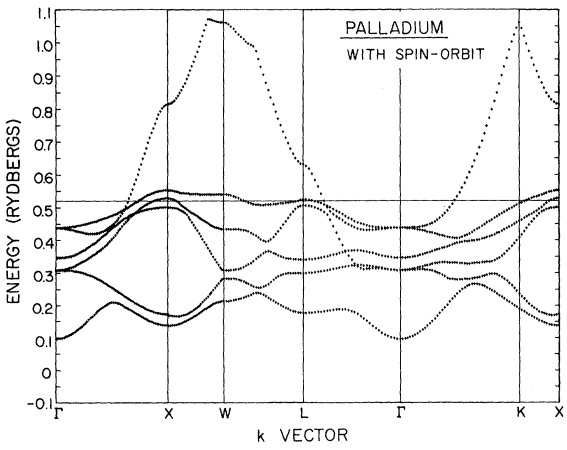

FIG. 5. Relativistic bands of palladium produced by the parameters of Table III. Along the line Γ to X, the bands show three intersections with the Fermi energy. As is discussed in text, the small fifth-band hole pocket near the point L is probably spurious.

IV. RESULTS

In this section, we discuss results derived from the APW bands of Sec. II as fit by the modified combined interpolation scheme.

A. Relativistic Band Structure and Density of States

The relativistic palladium band structure, derived from the parameters for the configuration $4d^{10}5s^0$ (HFS) and the spin-orbit coupling parameter found as described in the last section is presented in Fig. 5. Comparison of Fig. 5 with Fig. 1 shows that the addition of relativistic effects has split bands which were degenerate at a number of high-symmetry points of the Brillouin zone in the nonrelativistic case. In particular, the degeneracy of the $\Gamma_{25'}$ level has been split into the Γ_8^+ and Γ_7^+ levels, and the important degeneracy at X_5 has been lifted into the two levels X_7^+ and X_6^-.

Figures 6 and 7 give a histogram density of states of palladium derived from the bands shown in Figs. 1 and 5, respectively. A quadratic interpolation technique (QUAD)[33] was used to treat a million Monte Carlo points distributed in $\frac{1}{48}$ of the Brillouin zone. A histogram width of 0.001 Ry and a mesh size[33] of 10 were used. Integration of these histograms gives a Fermi energy which falls at 0.5246 Ry in the nonrelativistic case and at 0.5204 Ry in the relativistic case. Figure 8 shows a more accurate histogram of the region just around E_F for the relativistic case using a

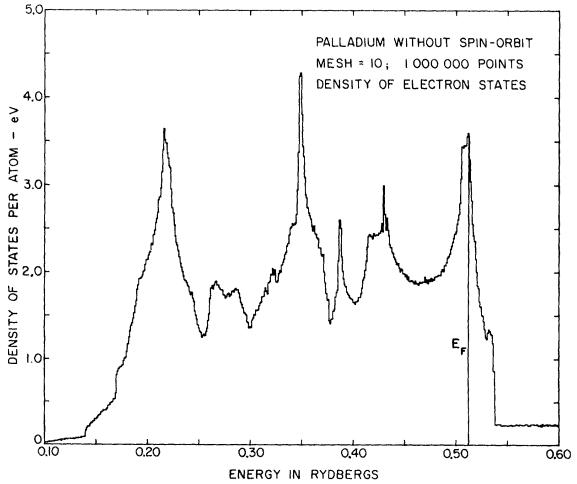

FIG. 6. Density of states of nonrelativistic palladium. Histogram was produced by the quad scheme, using histogram width of 0.001 Ry, and sampling 1 000 000 independent Monte Carlo points. Vertical accuracy is approximately 1%. Note that $N(E_F)$ for this calculation is much larger than that of Fig. 2.

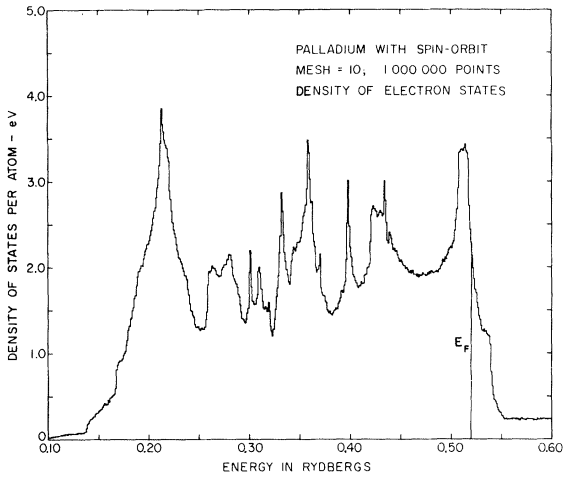

FIG. 7. Density of states of relativistic palladium. The histogram was produced by the QUAD scheme, using a histogram width of 0.001 Ry, and sampling 1 000 000 Monte Carlo points. Vertical accuracy is about 1%.

finer mesh size of 13. Because of the number of Monte Carlo points used, the histogram has a vertical accuracy of about 1%. This statistical noise is barely visible in the expanded scale density of states plotted in Fig. 8.

Figure 9 plots the density of states of Fig. 7 as a function of fractional electron concentration in order to allow easy comparison between our calculated curves and the results of alloy experiments. If the rigid-band model were applicable to the electronic structure of all the fcc transition metals, then Fig. 9 would provide a universal curve for the effective density of states. Deviations away from Fig. 9 in the experimental results indicate either breakdown of the rigid-band model or large energy-dependent enhancement effects. The results of Fig. 9 are accurate to perhaps 1–2%. The small peak near 12.0 electrons/atom is real and corresponds to the critical point structure associated with the (111) neck region in silver. Because the total number of electrons contained in the narrow peak above 0.5 Ry in Fig. 7 is large, this structure appears much broader when plotted as a function of concentration in Fig. 9.

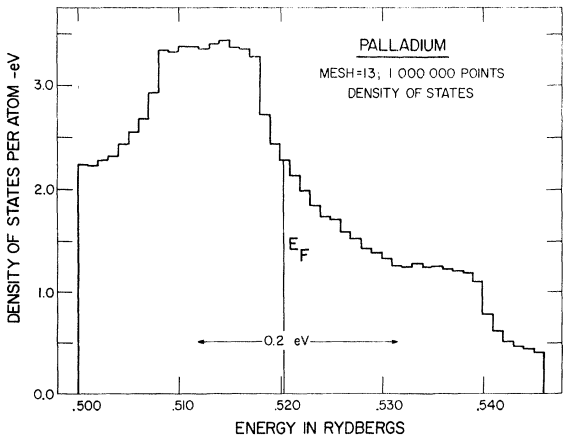

FIG. 8. Density of states of palladium in the immediate vicinity of the Fermi energy. Because the microscopic quadratic interpolation was carried out on a finer mesh in this calculation than the one used in Fig. 8, the rms vertical accuracy is somewhat better here. In particular, the single spike of width 0.001 Ry near $E=0.50$ Ry in Fig. 7 has disappeared.

Although the extrinsic accuracy of our density-of-states histograms is rather high, comparisons between our calculations and various experimental results must be made cautiously. In palladium, as shown in Fig. 9, the Fermi energy falls at a place on the density-of-states curve which has a steep first derivative. The Fermi energy can be placed to an accuracy of better than 0.0002 Ry by integrating $N(E)$ up to 10 electrons/atom. A better measure of the intrinsic accuracy of the bands is given by treating the Fermi energy as a variational parameter and by comparing our predicted results to a few experimental Fermi radii. The shifts in the Fermi energy obtained this way were about 0.001 Ry. This error represents the deviation of the predicted radii from experiment when E_F is found by integrating $N(E)$. The largest absolute error in Fermi radii is about 2%.

A least-squares procedure was used to fit the five points of our histogram in Fig. 8 which were closest to E_F to a four parameter function of the form

$$N(E) = A + BE + CE^2 + DE^3 \,. \tag{3}$$

From this fit we obtain the values 31.06, 2.28×10^3, and 2.11×10^5 for the zeroth, first, and second de-

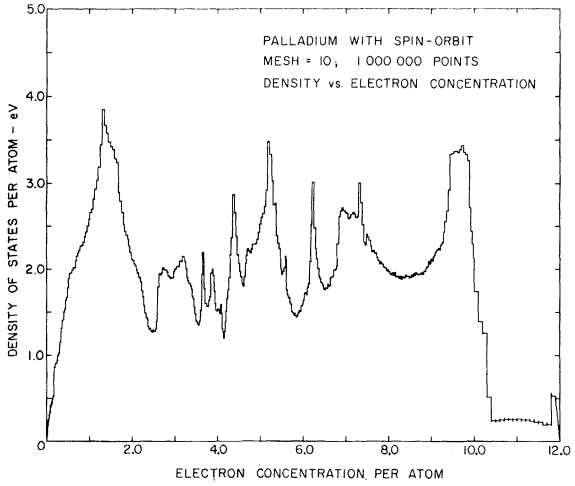

FIG. 9. Density of states of palladium plotted as a function of fractional electron concentration.

rivatives of the density of states, respectively, in Rydberg units. Because of the statistical fluctuation error of Monte Carlo calculations, the percentage accuracy of these derivatives is about 1, 9, and 75, respectively. The greater inaccuracy of the first and second derivatives occurs because they are formed essentially by taking differences of quantities with random deviations.

In addition to this purely statistical error, the limited energy resolution estimated above to be 0.001 Ry must be considered. The density of states and its derivatives could have any value appropriate to an energy $(E_F - 0.001) < E < (E_F + 0.001)$. The "true" density of states is assumed to be similar to our calculated density of states curve, but shifted to a new effective Fermi energy somewhere in this range. This shift could represent either a net change of position of d bands relative to s-p bands, or a net widening or narrowing of the d-band complex.

Taking both types of error into account, and assuming that the two errors are approximately independent, the total error is given by

$$\sigma_i^2 = \sigma_i^2(M) + \sigma_i^2(I), \tag{4}$$

where σ_i is the error of the ith derivative, $\sigma_i(M)$ the error due to Monte Carlo sampling, and $\sigma_i(I)$ the error due to the finite energy resolution. The final estimates for the density of states and its derivatives for palladium are

$$\begin{aligned} N(E_F) &= +2.281 \text{ states/eV atom} \pm 0.171, \\ N'(E_F) &= -12.3 \text{ states/(eV)}^2 \text{ atom} \pm 1.62, \\ N''(E_F) &= +84.0 \text{ states/(eV)}^3 \text{ atom} \pm 65.0, \end{aligned} \tag{5}$$

where we have converted to electron-volt units for convenience.

The Fermi energy (0.5204 Ry) and the density of states (31.06 electrons/atom Ry) of our relativistic bands are in (surprisingly) good agreement with those given before[8] (0.524 and 28.2, respectively) for the nonrelativistic bands and the regular-samples density of states (Fig. 2). The values are also close to those derived from the relativistic APW calculation of Andersen and Mackintosh,[18] who used full Slater exchange and a muffin-tin potential found from the configuration $4d^{10}$ for the Dirac-Slater atomic-charge density.[27] Andersen and Mackintosh found the Fermi energy by locating that constant energy contour which produced equal hole and electron volumes. Their Fermi energy of 0.515 Ry relative to Γ_1 represents a d-band complex approximately 0.1 Ry higher than ours. However, their density-of-states value of 32 states/atom Ry is in good agreement with ours. The agreement merely indicates that, in fcc transition metals, the structure in $N(E)$ near the top of the d-band complex is relatively insensitive to net shifts of the d bands relative to the plane-wave s-p bands. Transition metals in the $3d$ row of the Periodic Table show this insensitivity.[11]

B. Electronic Specific Heat, Magnetic Susceptibility, Effective g Values, and Many-Body Enhancement Effects

Two experimental quantities used to estimate the value of the density of states at the Fermi level are the electronic specific heat C_v, and the magnetic susceptibility χ. Since these experimental quantities are enhanced by different many-body effects, the usual procedure was reversed and our values, Eq. (5), were used to estimate the effective enhancements.

The enhancements of the specific heat were defined as

$$\gamma = R\gamma_0 = (1 + \alpha_e + \alpha_{ph} + \alpha_p)\gamma_0, \tag{6}$$

where γ is the experimental specific heat in density-of-states units, $\gamma_0 = N(E_F)$, and α_e, α_{ph}, and α_p are the enhancements due to electron-electron, electron-phonon, and paramagnon interactions, respectively. The changes in the self-energy induced by these three interactions were assumed to be additive. Although this assumption is not strictly true, Eq. (6) is sufficiently accurate for the qualitative arguments which follow below.

For the specific heat, Hoare *et al.*[1,2] obtained values of 9.41 mJ mole^{-1} deg^{-2}, or 55.0 electrons/atom Ry. More recently, Choteau *et al.*[34] obtained values of 9.40 mJ mole^{-1} deg^{-2}, or 54.9 electrons/atom Ry. This latest value yields a ratio $R = 1.76$, or a total enhancement $\alpha = R - 1 = 0.76$. The electron-electron and the electron-phonon interactions in palladium are also assumed to have roughly the same strength as deduced for superconducting transition metals,[35] i.e., $\alpha_e + \alpha_{ph} \simeq 0.35$. The large fraction, $\alpha_p = 0.41$, can then be attributed to paramagnons.[5] Although this value for α_p is smaller than many previous estimates, the effect of paramagnons is nonzero for the entire range of values given in Eq. (5). Assuming that $\alpha_e + \alpha_{ph} = 0.35$, the largest and smallest estimates of $N(E_F)$ given in Eq. (5) yield total enhancement ratios R of 1.65 and 1.91, and paramagnon enhancements of 0.30 and 0.56, respectively.

The static susceptibility χ has a larger percentage enhancement and is therefore perhaps a more favorable case for deriving enhancement ratios than the specific heat. We used the results of Foner *et al.*,[4] namely, a value of 6.91×10^{-6} electron emu/g for the susceptibility χ or a value of 312.0 for χ/μ_B^2 in electron/atom Ry units where μ_B is the Bohr magneton.

The paramagnon theory[5] states that appreciable exchange enhancement of the susceptibility of pure Pd is given by

$$\chi = D\chi_p = \chi_p (1 - \tfrac{1}{2}\chi_p V_0 \mu_B^{-2})^{-1} \quad , \tag{7}$$

where V_0 is an effective exchange interaction potential between the conduction electrons, and D is the Stoner-Wohlfarth enhancement factor. The unenhanced Pauli susceptibility is generally given as

$$\chi_p = \mu_B^2 N(E_F) \, , \tag{8}$$

where μ_B is the Bohr magneton, and $N(E_F)$ is the density of states for two spin states. The usual factor of 2 has been absorbed by the double spin $N(E_F)$.

In deriving Eq. (7), the g factor of the electrons was rigidly set equal to 2, the spin g factor. In palladium, the g factor of conduction electrons can deviate markedly away from 2. The states X are associated with the spin-orbit split levels X_7^+ and X_6^+ at the top of the d bands. Since the Fermi level in palladium passes very near to the X_7^+, X_6^+ levels, the spin mixing induced by the spin-orbit coupling alters the g factor over much of the Fermi surface. This is discussed in more detail in a forthcoming publication.

For every band n and point $\vec{k}$ an effective g factor $g_n(\vec{k})$ can be defined. Neglecting the small orbital angular momentum contribution, an infinitesimal magnetic field $\vec{H}$ adds a perturbation to the Hamiltonian of the form $H_p = \frac{1}{2}\mu_B \vec{\sigma} \cdot \vec{H}$, where $\vec{\sigma}$ are the Pauli matrices. The infinitesimal perturbation lifts the Kramers degeneracy of the level $E_n(\vec{k})$, giving the energies

$$E_n^{\pm}(\vec{k}) = E_n(\vec{k}) \pm \tfrac{1}{2} g_n(\vec{k}) \, \mu_B |\vec{H}| \, . \tag{9}$$

Equation (9) is an implicit definition of $g_n(\vec{k})$. The term $g_n(\vec{k})$ depends on the vector direction of the external magnetic field $\vec{H}$. The change in occupation number induced by (31) is given by

$$\Delta f_n(\vec{k}) = f[E_n^-(\vec{k})] - f[E_n^+(\vec{k})] \, , \tag{10}$$

where f is the Fermi function

$$f(E_n^{\pm}(\vec{k})) = (\exp\{[E_n(\vec{k}) \pm \tfrac{1}{2} g_n(\vec{k}) \, \mu_B |\vec{H}| - E_F]/KT\} + 1)^{-1}, \tag{11}$$

E_F is the Fermi energy, T is the temperature, and K is Boltzmann's constant. With the effective magnetic moment of the nth band at $\vec{k}$

$$m_n(\vec{k}) = \tfrac{1}{2} g_n(\vec{k}) \, \mu_B \, , \tag{12}$$

the total magnetic moment M induced by Eq. (9) is

$$M = \textstyle\sum_n [1/(2\pi)^3] \int d\vec{k} \; m_n(\vec{k}) \, \Delta f_n(\vec{k}) \, . \tag{13}$$

Taking the limits of zero temperature and small external magnetic field,

$$M = \left(\frac{\mu_B}{2}\right)^2 H \sum_n \frac{1}{(2\pi)^3} \times \int d\vec{k} \; g_n(\vec{k}) \, g_n(\vec{k}) \left(\frac{\partial f}{\partial E_n(\vec{k})}\right)_{[E_n(\vec{k}) = E_F]} . \tag{14}$$

This expression can be separated into an effective g factor and the density of states:

$$M = (\tfrac{1}{2}\mu_B)^2 H g^2_{\text{eff}} N(E_F), \tag{15}$$

where

$$g^2_{\text{eff}} = [2/N(E_F)] \textstyle\sum_n \int d\vec{k} \; g_n^2(\vec{k}) \; \delta(E_n(\vec{k}) - E_F). \tag{16}$$

Because palladium is a cubic material, M is a scalar quantity and is independent of the vector direction of $\vec{H}$. The quantity g^2_{eff} is also a scalar, but the quantity $g_n(\vec{k})$ is not a scalar, but a second-rank tensor.

The Pauli susceptibility Eq. (8) must be modified to

$$\chi_p = (\tfrac{1}{2}\mu_B)^2 \, g^2_{\text{eff}} \, N(E_F) \tag{17}$$

or $\chi_p = (\mu')^2 N(E_F)$,

where μ' is an effective magnetic moment

$$\mu' = \tfrac{1}{2} g_{\text{eff}} \, \mu_B \, . \tag{18}$$

Averages over a few $\vec{k}$ points on the three sheets of the Fermi surface suggest that the presence of strong d-state spin-orbit coupling has reduced g_{eff} in palladium from 2.00 to the value $g = 1.65$.

Placing Eqs. (18) and (5) in Eq. (7) gives estimates for D of

$$\begin{aligned} D &= 14.80 \quad g = g_{\text{eff}} = 1.65 \\ &= 10.05 \quad g = 2.00 \, . \end{aligned} \tag{19}$$

However, based on our range of values 33.3–28.7 for the density of states $N(E_F)$, and assuming a constant g_{eff} of 1.65, a range (13.8)–(16.0) is obtained as an estimate of D.

In calculating the RPA susceptibility, the Pauli susceptibility enters the denominator of D. Therefore, when V_0 is found from Eq. (7) using $\mu' = \mu_B$, such estimates of the effective exchange interaction constant V_0 should be increased by a factor of $(2/g_{\text{eff}})^2$. If D was found from Eq. (7) using an estimated value of V_0, then such an estimated V_0 should be reduced by $(\frac{1}{2}g_{\text{eff}})^2$. Alternatively, the rescaling of a calculated V_0 by this factor using $g_{\text{eff}} = 1.65$ reduces a D previously estimated to be 20 to the smaller value of 2.82.

The experimental static susceptibility is sensitive both to temperature and to external magnetic fields.[12] The data of Foner *et al.*[4] were taken at low temperature and essentially low external magnetic fields. Because of the large Stoner factor

($D \sim 15$), the usual temperature dependence of the unenhanced susceptibility must be modified to include higher-order terms. The temperature dependence is usually given by

$$\chi_p(T) = \chi_p(0)\,[(1 + \tfrac{1}{6}\pi^2 \nu_0 K^2 T^2)], \tag{20}$$

$$\text{where } \nu_0 = \frac{N''(E_F)}{N(E_F)} - \left(\frac{N'(E_F)}{N(E_F)}\right)^2 . \tag{21}$$

A short calculation for $D \gg 1$ so that $\frac{1}{2}\chi_p(0) \times V_0 \mu_B{}^{-2} \sim 1$ for T^2 small gives

$$\chi(T) = D\chi_p(0)\,(1 + \pi^2 \nu_0 K^2 T^2 + D\tfrac{1}{6}\pi^2 \nu_0 K^2 T^2) , \tag{22}$$

where the third term completely dominates the second for our value of D.

The magnetic field dependence of the enhanced susceptibility has been given by Wohlfarth[12] as

$$\chi(H) = D\chi_p(0)\,(1 + \beta H^2) , \tag{23}$$

$$\text{where} \quad \chi_p(0) = (\tfrac{1}{2}g)^2 \mu_B^2 N(E_F), \tag{24}$$

$$\beta = 1/2\nu\,(\tfrac{1}{2}g)^2 \mu_B^2 D^3 , \tag{25}$$

$$\text{and} \quad \nu = \frac{N''(E_F)}{N(E_F)} - 3\left(\frac{N'(E_F)}{N(E_F)}\right)^2 . \tag{26}$$

Our values [Eq. (5)] for the derivatives of the density of states of palladium give

$$\nu_0 = +1.59 \times 10^3 \text{ states/atom Ry}^2 \quad \text{or} \quad +8.3 \text{ states/atom (eV)}^2 \tag{27}$$

$$\text{and } \nu = -1.65 \times 10^4 \text{ states/atom Ry}^2 \quad \text{or} \quad -89.4 \text{ states/atom (eV)}^2 . \tag{28}$$

Because of the large uncertainty in $N''(E_F)$, perhaps only the signs of Eqs. (27) and (28) are known.

Since the sign of ν_0 is positive, we predict a quadratically increasing $\chi(T)$ in the low-T region. Fitting the experimental data[4] found below 50 °K to a quadratic form $A + BT^2$ yields an experimental value of

$$\nu_0' = +1.12 \times 10^2 \text{ eV}^{-2} \tag{29}$$

which is in fair agreement with Wohlfarth's[12] estimate:

$$\nu_W = 1.18 \times 10^{+26} \text{ erg}^{-2} = +3.02 \times 10^2 \text{ eV}^{-2} . \tag{30}$$

Our value of ν_0 is an order of magnitude smaller than ν_0'. However, our mean values for terms of ν_0, N'' versus $(N')^2$, almost completely cancel. For example, the value of N'' could be doubled and still remain within our error range with the result that the comparison to ν_0' is then greatly improved.

A better procedure is to use ν_0' and our values of ν, $N'(E_F)$ and $N(E_F)$ to fix $N''(E_F)$. This gives an improved value

$$N''(E_F)_i = +142 \text{ eV}^{-2} . \tag{31}$$

Placing this value back in Eq. (26) yields an improved value of ν,

$$\nu_i = +0.52 \times 10^2 \text{ eV}^{-2} \tag{32}$$

$$\text{or} \quad \rho = \nu_i/\nu_W = 0.17 . \tag{33}$$

The nomograph given in Fig. 2 of Ref. 36 shows that values $\rho = 0.17$ and $D = 14.8$ to be (barely) consistent with the measured high-field susceptibility $\chi(H)$.

C. Fermi Surface

Figure 10 shows the intersection of the relativistic Fermi surface with the principal symmetry planes of the fcc lattice using the Fermi energy obtained from $N(E)$. The surface consists of the same three sheets with the same connectivity as was previously obtained[8] by means of nonrelativistic APW bands. However, changes induced in the band structure by the spin-orbit coupling have changed the details of the three sheets. In particular, the Γ-centered sixth-band electron sheet now contains 0.36 electrons/atom, rather than 0.39 obtained by the nonrelativistic interpolation scheme fit. The three small X-centered fourth-band hole pockets now contain 0.0031 holes/atom, compared to an experimental value of 0.003. The large jungle-gym fifth-band hole surface now contains 0.36 holes/atom, compared to 0.39. Thus the addition of spin-orbit coupling to the nonrelativistic band structure has brought the Fermi-surface volumes into good agreement with the volumes based on dHvA data.

Also shown in Fig. 10, as a dashed surface, is a small L-centered fifth-band hole pocket. We believe that the existence of this pocket in palladium is unlikely since it has not been seen in the dHvA effect. The present L-centered pocket has a (111) orbital mass of 0.56 electron masses, a $(\bar{1}\bar{1}2)$ orbital mass of 0.95 electron masses and

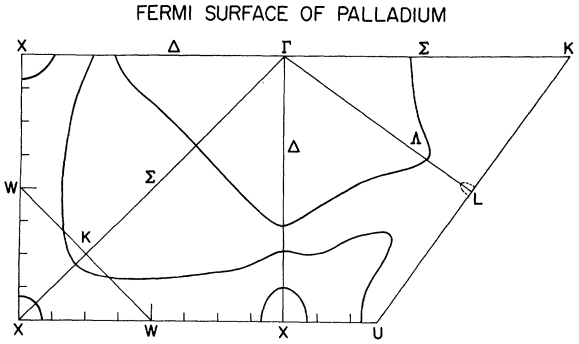

FIG. 10. Fermi surface of palladium produced by the combined interpolation scheme. Intersection points along symmetry lines are given in Fig. 5. Fermi energy was found by integrating the curve in Fig. 7 up to 10 electrons/atom.

contains a total of 0.884×10^{-3} carriers in the first Brillioun zone (Bz) in eight half-ellipsoids. A similar pocket does exist in rohdium. The lack of any dHvA evidence for this sheet in palladium suggests that either the effective-mass enhancement on this sheet is of the order of 4–5, or the Fermi energy near the point L lies 0.0027 Ry higher than we have placed it by integrating $N(E)$ up to electrons/atom. The independent theoretical calculations of Andersen and Mackintosh also suggest the existence of an L-centered pocket, but they also believe, on the basis of the lack of dHvA data, that the L-centered pocket is unlikely.

Table IV shows a few symmetry-plane radii of the Γ-centered sheet of the palladium Fermi surface. These radii are compared with the experimental data[37] and the theoretical radii produced by Andersen and Mackintosh.[18] The agreement among the three sources is good. Apparently one-electron band-structure models can accurately reproduce the complicated Fermi-surface geometrics for palladium.

TABLE IV. Fermi-surface radii for the Γ-centered sheet of palladium in atomic units.

Direction	Experiment KWH[a]	Theory AM[b]	Theory Present
[100]	0.585	0.578	0.546
[110]	0.426	0.423	0.419
[111]	0.593	0.616	0.568

[a]L. R. Windmiller, J. B. Ketterson, and S. Hornfeldt, in Ref. 37.

[b]O. K. Andersen and A. R. Mackintosh, in Ref. 18.

V. SUMMARY AND CONCLUSIONS

A detailed investigation of the electronic structure of palladium was made in terms of two different band models – the *ab initio* APW method and the semiempirical combined interpolation scheme. The sensitivity of the energy bands of palladium to the details of the assumed one-electron potential, especially with regard to configuration and exchange, was seen by examining the bands produced by three different potentials. The width and position of the d-band complex were found to be particularly sensitive features of the band structure of palladium.

Those APW bands produced by the $4d^{10}5s^{0}$ (HFS) potential were taken as a starting point, and spin-orbit coupling was added to the d bands so as to reproduce a few critical dHvA areas. From these relativistically augmented energy bands a highly accurate density of states was calculated. The Fermi energy was found by integrating this density of states up to 10 electron states/atom. From the value of the Fermi energy, Fermi radii were derived from the relativistic energy bands. The calculated radii were found to be in good agreement with experimentally determined radii.

On the basis of our results several conclusions may be reached about the electronic structure of palladium. The only adjustment made of the energy bands used the dHvA data to adjust the value d spin-orbit coupling. The good agreement obtained between experimental radii and calculated values shows that Fermi-surface radii of complicated transition metals can be accurately predicted within one-electron models. Better agreement than that achieved here would require either deepening our understanding of the electronic structure of transition metals by going beyond the single-particle model, or, within the one-electron framework, adjusting the energy so as to obtain agreement with high precision experiments. At present, detailed radii of all sheets of the Fermi surface of palladium are not available in the literature, although results for the Γ-centered sheet should be published shortly.[37,38] The adjustment of the energy bands to fit experiment could take two forms: either in terms of parameters for the combined interpolation scheme as above, or in terms of parameterizing phase shifts or logarithmic derivatives within a first-principle band-structure method. Before using the latter scheme, however, it is important to know in detail the effects on the electronic energy bands of the potential in the region outside the muffin-tin spheres.[39]

Within the single-particle picture good agreement was also obtained with the observed Fermi-surface electron and hole volumes of 0.36 electrons/atom. This value differs substantially from the value of 0.56 electrons/atom deduced from specific-heat and susceptibility experiments on the Pd-Ag alloy system. This may indicate that the rigid-band model breaks down for these alloy systems. We hope to return to this problem in the future.

From our single-particle results and the experimental data, estimates were derived for many-body enhancement effects at the Fermi energy. These enhancements are in good agreement with those derived from the preliminary version of this paper.[8] Because of the strong effects of spin-orbit coupling on the effective g factor, our estimate for the enhancement of the static susceptibility of palladium is nearly 50% higher than our previous estimate. Moreover, we believe that due to strong s-d hybridization, the anisotropy of the effective g factor for electrons near the Fermi energy is substantial.

The strong g-factor anisotropy of the energy bands exhibited at the Fermi energy should profoundly affect the single-particle transverse sus-

ceptibility $\chi_{\uparrow\downarrow}(q, \omega)$. Moreover, the effective anisotropy fields due to spin-orbit coupling should strongly affect both the lifetime and frequency of spin fluctuations in palladium. To our knowledge, these strong effects have not been included in any theoretical treatment of spin fluctuations except in terms of averages. Detailed calculations are now in progress.

One result of our work is the great similarity between the two density-of-states curves, Figs. 6 and 7, calculated with and without spin-orbit coupling. Since the connectivity and separation of the underlying band structures, Figs. 1 and 5, are rather profoundly modified by the presence or absence of spin-orbit coupling, changes were anticipated in the resulting density of states. A detailed examination of Figs. 6 and 7 shows that the largest differences are in the middle of the d-band complex, rather than at either the top or bottom ends. Thus, although the addition of spin-orbit splitting lifts the degeneracy of the two levels X_5 and L_3 of the nonrelativistic calculation and alters Fermi-surface dimensions profoundly, it does not greatly modify the calculated density of states.

Recently, Eastman[16] has calculated an approximate optical density of states from our final $N(E)$, Fig. 7. He assumed that optical-excitation matrix elements were constant and that elastic scattering and lifetime-broadening effects could be simulated by a term proportional to $(E - E_F)$. The four resulting pieces of structure in his optical density-of-states curve compared well with the four pieces of structure in the photoemission data except that the theoretical curve was narrower by about 15%. Eastman's work suggests two possibilities: Our d band may be approximately 15% too narrow, implying that our estimate of enhancement effects must be increased by 15%. On the other hand, systematic effects excluded in his theoretical calculation may shift structure in the optical density of states produced by photoemission experiments away from single-particle results. Both possibilities deserve further study.

ACKNOWLEDGMENTS

We would like to thank the staffs of the Applied Mathematics Division at Argonne National Laboratory and the Computation Center at Massachusetts Institure of Technology for excellent service, Miss Martha Katzin and Mrs. Ruth Sheshinsky for programming assistance, Dr. O. K Anderson, Dr. D. E. Eastman, Dr. S. Foner, Dr. S. Hornfeldt, Dr. J. B. Ketterson, Dr. A. R. Mackintosh, Dr. R. E. Watson, and Dr. L. R. Windmiller for helpful discussions and K. L. Mueller for editorial service.

APPENDIX A: SPIN-ORBIT COUPLING IN OPW BLOCKS

Here we discuss the spin-orbit coupling corrections to the d-OPW and the OPW-OPW blocks. The d-OPW block can be treated much more simply than the d-d block discussed above. Here the terms of interest have the form $\vec{\sigma}\cdot\vec{T}(\vec{k})$ where $\vec{T}(\vec{k})$ is given by

$$\vec{T}(\vec{k}) = \langle d|\lambda\vec{L}|\vec{k}\rangle - \sum_{d'}\langle d|\lambda\vec{L}|d'\rangle\langle d'|\vec{k}\rangle \ . \qquad \text{(A1)}$$

We assume that $\langle d|L_z = (-1)^m|m|\langle d|$, where m is the magnetic quantum number of d. Considering the z component of Eq. (A1) and letting the $\vec{L}$ operate to the left gives

$$T_z(\vec{k}) = (-1)^m|m|[\langle d|\lambda|\vec{k}\rangle - \langle d|\lambda|d'\rangle\langle d'|\vec{k}\rangle] \ . \qquad \text{(A2)}$$

Also, the m quantum number of d' = the m quantum number of d; however, the states can have different radial dependences. As before, Eq. (A2) can be restricted to zeroth-neighbor terms alone. An estimate for the size of T_z is obtained by approximating both the band-radial d-wave function and the effective potential in Eq. (A2) by atomic[27] values. The result is k dependent and its largest value (0.0043 Ry) occurs at $k = 4.16$ atomic units. This value is far outside the first Brillouin zone of palladium; thus, the effects of Eq. (A2) occur only in higher bands. The fact that the maximum occurs at such a large k value merely reflects the fact that the radial peak of the integrand of Eq. (A3), $R_d(r)\lambda(r)$, occurs at small r. In any event, $T_z(\vec{k})$ is sufficiently small for all $\vec{k}$ that T_z can be set equal to zero.

In the OPW-OPW block occur terms similar to Eq. (A1). In the Hamiltonian is an additional term of the form $\vec{\sigma}\cdot\vec{P}(\vec{k}, \vec{k}')$, where $\vec{P}(\vec{k}, \vec{k}')$ depends on both the initial and final $\vec{k}$ vector of the OPW's. We write $\vec{P}(\vec{k}, \vec{k}')$ as the sum of two terms

$$\vec{P}(\vec{k}, \vec{k}') = \vec{Q}(\vec{k}, \vec{k}') + \vec{R}(\vec{k}, \vec{k}') , \qquad \text{(A3)}$$

where Q is given by

$$\vec{Q}(\vec{k}, \vec{k}') = \langle\vec{k}|\lambda\vec{L}|\vec{k}'\rangle + \sum_{c, c'}\langle\vec{k}|c\rangle\langle c|\lambda\vec{L}|c'\rangle\langle c'|\vec{k}'\rangle \qquad \text{(A4)}$$

and by

$$\vec{R}(\vec{k}, \vec{k}') = \sum_c -\langle\vec{k}|\lambda\vec{L}|c\rangle\langle c|\vec{k}'\rangle - \langle\vec{k}|c\rangle\langle c|\lambda\vec{L}|\vec{k}'\rangle, \qquad \text{(A5)}$$

where the sum is over all the core states plus the $4d$ states. Again we examine the z component of Eq. (A3). By symmetry the explicit double sum over c and c' in Eq. (A4) may be reduced to a single sum and the implicit sum over neighbors may be reduced to zeroth neighbors alone. Then, setting $L_z|c\rangle = m|c\rangle$,

$$Q_z(\vec{k}, \vec{k}') = \langle\vec{k}|\lambda L_z|\vec{k}'\rangle + \sum_c m\langle\vec{k}|c\rangle\langle c|\lambda|c\rangle\langle c|\vec{k}'\rangle \qquad \text{(A6)}$$

and

$$R_z(\vec{k},\vec{k}') = -\sum_c m(\langle\vec{k}|\lambda|c\rangle\langle c|\vec{k}'\rangle + \langle\vec{k}|c\rangle\langle c|\lambda|\vec{k}'\rangle). \tag{A7}$$

A Rayleigh expansion of both $\langle\vec{k}|$ and $|\vec{k}'\rangle$ gives

$$|\vec{k}'\rangle = 4\pi\sum_{l\mu} i^l j_l(k'r)\, Y_l^{\mu*}(\hat{k}')\, Y_l^{\mu}(\hat{r}) \tag{A8}$$

and

$$\langle\vec{k}| = 4\pi\sum_{l'\mu'}(-i)^{l'} j_{l'}(kr)\, Y_{l'}^{\mu'}(\hat{k})\, Y_{l'}^{\mu'*}(\hat{r}). \tag{A9}$$

Placing Eqs. (A8) and (A9) in Eqs. (A6) and (A7),

$$Q_z(\vec{k},\vec{k}') = 16\pi^2\sum_{l,m} m Y_l^m(\hat{k}')\, Y_l^{m*}(\hat{k})\cdot(\langle\vec{k}|\lambda|\vec{k}'\rangle + \langle\vec{k}|c\rangle\langle c|\lambda|c\rangle\langle c|\vec{k}'\rangle), \tag{A10}$$

and

$$R_z(\vec{k},\vec{k}') = -16\pi^2\sum_{l,m} m Y_l^m(\hat{k}')\, Y_l^m(\hat{k}) \times(\langle\vec{k}|\lambda|c\rangle\langle c|\vec{k}'\rangle + \langle\vec{k}|c\rangle\langle c|\lambda|\vec{k}'\rangle), \tag{A11}$$

where all of the integrals of Eqs. (A10) and (A11) are wholly radial and both $|\vec{k}\rangle$ and $|c\rangle$ carry quantum numbers l and m implicity. Adding Eqs. (A10) and (A11) gives

$$P_z(\vec{k},\vec{k}') = 16\pi^2\sum_{l,m} m Y_l^m(\hat{k}')\, Y_l^{m*}(\hat{k}) + (\langle\vec{k}|\lambda|\vec{k}'\rangle + \langle\vec{k}|c\rangle\langle c|\lambda|c\rangle\langle c|\vec{k}'\rangle - \langle\vec{k}|\lambda|c\rangle\langle c|\vec{k}'\rangle - \langle\vec{k}|c\rangle\langle c|\lambda|\vec{k}'\rangle). \tag{A12}$$

The inclusion of the factor m inside the sum dramatically changes the symmetry properties of Eq. (A12) from those usual in the interpolation scheme. In particular Eq. (A12) is factorizable into components of constant l,

$$P_z(\vec{k},\vec{k}') = \sum_l P_z^l(\vec{k},\vec{k}'). \tag{A13}$$

To examine the symmetry properties, we list the first few terms of Eq. (A13):

$$\begin{aligned} P_z^0(\vec{k},\vec{k}') &= 0,\\ P_z^1(\vec{k},\vec{k}') &= \alpha(\vec{k},\vec{k}')(\hat{k}\times\hat{k}'),\\ P_z^2(\vec{k},\vec{k}') &= \beta(\vec{k},\vec{k}')(\vec{k}\times\vec{k}')(\vec{k}\cdot\vec{k}'), \end{aligned} \tag{A14}$$

where α and β are radial form factors. The angular dependence of (A14) is governed entirely by the cross- and dot-product terms of $\vec{k}$ and $\vec{k}'$. The cross product $(\hat{k}\times\hat{k}')$ enters all terms[28] and makes $P_z(\vec{k},\vec{k}')$ a wholly nondiagonal interaction term. Explicit wave functions and form for $\lambda(r)$ again show that the terms represented by Eq. (A14) are sufficiently small that they can be replaced by zero.

The term $\alpha(\vec{k},\vec{k}')$ has a maximum value of 0.0013 Ry at $|\vec{k}| = |k'| = 3.4$ a.u. and the term $\beta(\vec{k},\vec{k}')$ has a maximum value of 0.0004 Ry at $|\vec{k}| = |\vec{k}'| = 11.3$ a.u. As before the effective integrands of Eq. (A14) are steeply peaked for small r so that both α and β have their peak value at large k, k'.

APPENDIX B: TECHNIQUE USED TO FIND PARAMETERS

The combined interpolation scheme uses 12 parameters given in Table III. At least two of these parameters (R_0 and R_1) enter into the band-energy eigenvalues in a distinctly nonlinear fashion. Thus, a method was needed quickly to find a relatively large and unique set of parameters.

For a given set of values for the parameters, the model Hamiltonian can be diagonalized at any given point $\vec{k}$ of the Brillouin zone. The diagonalization yields a set of band-energy eigenvalues $E_p^n(\vec{k})$, where the subscript indicates that the eigenvalues come from the interpolation scheme with a set of parameters $\vec{p}$, a vector whose components label the various parameters. At this same point $\vec{k}$, APW band levels $E_A^n(\vec{k})$ also exist. The average or rms deviation of our results from the APW results at the point $\vec{k}$ is given by

$$D^2(\vec{k},\vec{p}) = (1/N)\sum_n [E_A^n(\vec{k}) - E_p^n(\vec{k})]^2, \tag{B1}$$

where D is written as a function of our vector of parameters and the total number of levels fit is N. These results are for one $\vec{k}$ point. However, a measure of the deviation of the two-band structures over the whole Brillouin zone is needed. Ideally this measure could be produced by integrating Eq. (1) over the Brillouin zone to define

$$D^2(\vec{p}) = (1/\tau)\int d\vec{k}\, D^2(\vec{k},\vec{p}), \tag{B2}$$

where τ is the volume of the first Brillouin zone. Placing Eq. (B1) into Eq. (B2) gives the zone-averaged deviation

$$D^2(\vec{p}) = (1/N\tau)\sum_n \int dk\, [E_A^n(\vec{k}) - E_p^n(\vec{k})]^2. \tag{B3}$$

The best parameter set $\vec{p}$ would fulfill the equation $D^2(\vec{p}) = 0$. Since fits achieved with the interpolation scheme are never perfect, the condition $D^2(\vec{p}) = 0$ is never fulfilled. Thus the best sets of parameters are those which make Eq. (B3) minimal. These parameters fulfill the condition that

$$\vec{\nabla}_{\vec{p}} D^2(\vec{p}) = 0, \tag{B4}$$

i.e., that the gradient of the deviation taken with respect to the parameter space is zero. If $D^2(\vec{p})$ had no minima, if $D(\vec{p})$ had a saddle point, or if several different minima [perhaps related by the partial inversion $D^2(\vec{p}) = D^2(-\vec{p})$] existed, a set of 12 unique parameters would be impossible to obtain.

Five parameters affect only the d bands. At a general point k a given d energy level can be a rather complicated function of these parameters. However, the matrix elements of the d block of

the Hamiltonian may be viewed as appropriately symmetrized Fourier series. A deviation function was chosen which was defined, not as an average over all points as in Eq. (B3), but only over points on symmetry lines. Many of the d-block matrix elements are then zero by symmetry, and for such points the energy levels become simple linear combination of the parameters. If only such points and levels are used,

$$E_{\vec{p}}^{n}(\vec{k}_s) = \sum_i A_i^n(\vec{k}_s) p_i \ , \tag{B5}$$

where k_s is a special symmetry point. The $A_i^n(\vec{k})$ are complicated functions of sines, cosines, and band indices, but are independent of the parameters p_i. The sum on i is restricted to only the five parameters which are involved in the d-d block of the Hamiltonian. A sufficient number of such special points $\vec{k}_s$ and levels n (total 5) allows us to invert Eq. (B5) to find unique values for the parameters.

However, both the original APW energy levels on the left-hand side of Eq. (B5) and the expansion coefficients on the right-hand side of Eq. (B5) contain various errors. Moreover, the d-d block of the model Hamiltonian has been truncated to include only first-neighbor terms. Thus, the set of parameters p_i which satisfies Eq. (B5) alone would probably not best minimize Eq. (B3). To obtain the best over-all fit, Eq. (B5) must be augmented by further points and levels.

After some trial and error the following procedure emerged:

(1) From all of the possible points in the Brillouin zone a special set of 10 were selected whose eigenvalues lie within an energy range given by Γ_1 to $X_{4'}$. The 10 points were five principal symmetry points Γ, X, L, W, and K; three midpoints on the three principal symmetry lines $\frac{1}{2}(\Gamma+X)$, $\frac{1}{2}(\Gamma+L)$, and $\frac{1}{2}(\Gamma+K)$; and two midpoints on the symmetry lines of the edges of the Brillouin zone $\frac{1}{2}(X+W)$ and $\frac{1}{2}(L+W)$.

(2) The point deviation [Eq. (B1)] was used to define the total deviation

$$D_s^2(\vec{p}) = (1/10) \sum_{\vec{k}_i} D^2(\vec{k}_i, \vec{p}) \ , \tag{B6}$$

where the sum is taken over the special set of 10 points.

(3) Initially all the parameters p_i were set equal to their copper values[11] except for d_0, the zero of energy of the d-band complex relative to the plane-wave bands. The zero of energy of the plane waves had been fixed so that Γ_1 (scheme) $= \Gamma_1$ (APW). The parameter d_0 was adjusted until the deviation, as calculated by Eq. (B6), was minimal.

(4) The shape of all the APW d bands is similar to the shape of those of copper except that the d-band width in palladium is about twice that of copper. For this reason a width parameter α was defined which rescaled the copper d-band parameters by means of the relations

$$\begin{aligned} dd\sigma(\mathrm{Pd}) &= \alpha \ dd\sigma(\mathrm{Cu}) \ , \\ dd\pi(\mathrm{Pd}) &= \alpha \ dd\pi(\mathrm{Cu}) \ , \\ dd\delta(\mathrm{Pd}) &= \alpha \, dd\delta(\mathrm{Cu}) , \end{aligned} \tag{B7}$$

and by $dd\pi_1 = dd\pi_2$,

where $dd\pi_1$ and $dd\pi_2$ are the two new parameters in Table III. The parameter α was then adjusted to make the deviation Eq. (B6) minimal.

(5) The effects of hybridization and orthogonality were also expected to scale roughly. A parameter β was defined such that

$$\begin{aligned} A(\mathrm{Pd}) &= \beta \ A(\mathrm{Cu}) \ , \\ B(\mathrm{Pd}) &= \beta \ B(\mathrm{Cu}) \ . \end{aligned} \tag{B8}$$

Again the β parameter was adjusted until the deviation of Eq. (B6) was minimal.

(6) From these values of d_0, α, and β, and from the parameters of copper the initial set of palladium parameters p_i were defined. The parameters p_i were varied individually by the amount v_i in Table III and in each case the minimum was found by computing one component of the gradient, Eq. (B4), and using a quadratic approximation to define D.

The order of the parameters for the variational routine was R_1, B, R_0, A, V_{111}, V_{200}, γ, $dd\delta$, $dd\pi_2$, $dd\pi_1$, $dd\sigma$, d_0. This routine was continued until no significant (0.0001 Ry) further improvement could be achieved in minimizing D.

This parameter procedure rapidly gave one unique set (p_i) for each APW band structure defined at the 10 special points. To further test for uniqueness the parameters A and B were replaced by $-A$ and $-B$, respectively, since the sign of these parameters is unknown. In this test the variational procedure given above reversed the initial signs to correspond to those given in Table III. To test the sign of the rest of the parameters the d-band parameters were inverted. The shape of the d band also inverted showing that the initial sign was correct. Two of the parameters, R_0 and R_1, do not have a unique sign. Since the even-order spherical Bessel functions are even, the hybridization and orthogonality terms are invariant to reversal of the signs of their arguments. We arbitrarily chose the positive sign for these parameters.

Table III lists the value of the deviation from the APW results of the fitted bands calculated at the 10 selected points. The parameters found from the 10 selected points were used to calculate the

deviation over all 89 points of the $4d^{10}5s^0$ (HFS) calculation. The rms error calculated this way was 0.0061 for the 89 points. The similarity of this value to that of the 10-point deviation function (0.0048) suggests that the parameters produced by minimizing the deviation at the 10 selected points are representative of the values which would be found from minimizing Eq. (B3). The combined interpolation scheme can therefore accurately interpolate band structure found from first a few points on the special symmetry lines into the bulk of the Brillouin zone.

As a final test of the accuracy of the fitted band structure, Fig. 1 compares the APW results for the $4d^{10}5s^1$ (HFS) potential and the interpolated bands. As expected from the small over-all deviation (0.005 Ry), the fitted bands follow the APW results closely. The largest consistent errors in the fitted bands occur in the second and third bands along Δ, in the second band along Z, and in the fourth and sixth band along Σ. In the regions where the first two errors occur, the states are wholly d-like so that these errors are probably caused by the truncation of the d-d block overlap parameters at first-neighbor terms alone. Inclusion of higher-neighbor terms should reduce these deviations.

The deviations along Σ are probably caused by the simple approximations used for the radial parts of the terms $\langle d|H|k\rangle$ and $\langle d|k\rangle$, namely, $Aj_2(kR_0)$ and $Bj_2(kR_1)$, respectively, and truncation of the d-d block. Both the form of the Hamiltonian and the typical energy eigenvalues plotted in Fig. 2 of Ref. 11 indicate that the energy of the sixth band depends on the sum and the difference of the hybridization and orthogonality terms. The errors appear largest along Σ since there are two d states with Σ_1 symmetry, the same symmetry as the lowest plane-wave state. Since each OPW-d interaction has about the same effective error, two such interactions would have about twice this average error. In all three of the fitted band structures, the error was, in fact, about double. The fit along Σ could probably be improved by using more sophisticated representations for $\langle d|H|k\rangle$ and $\langle d|k\rangle$ and further d-d overlap terms.

Both of the corrections indicated above could be included within the scheme without great difficulty. However, more parameters would be needed and much of the scheme's simplicity would be lost. The results achieved within the simple framework are sufficiently accurate for present needs.

---

*Work supported by the U. S. Atomic Energy Commission.

†Work supported in part by Advanced Research Project Agency through the Northwestern Materials Science Center.

‡Supported by the U. S. Air Force Office of Scientific Research.

§Operated with support from the U. S. Air Force.

[1]F. E. Hoare and J. C. Matthews, Proc. Roy. Soc. (London) A212, 137 (1952); J. Wucher, Compt. Rend. 242, 1143 (1956).

[2]F. E. Hoare and B. Yates, Proc. Roy. Soc. (London) A240, 42 (1957).

[3]A. M. Clogston, B. T. Matthias, M. Peter, H. J. Williams, E. Corenzwit, and R. C. Sherwood, Phys. Rev. 125, 541 (1962); A. I. Schindler and M. J. Rice, *ibid.* 164, 759 (1967), and references therein.

[4]S. Foner, R. Doclo, and E. J. McNiff, Jr., J. Appl. Phys. 39, 551 (1968).

[5]N. F. Berk and J. R. Schrieffer, Phys. Rev. Letters 17, 433 (1966); S. Doniach and S. Englesberg, *ibid.* 17, 750 (1966).

[6]N. E. Alekseevskii, G. É. Karstens, and V. V. Mozhaev, Zh. Eksperim. i Teor. Fiz. 46, 1979 (1964) [Soviet Phys. JETP 19, 1333 (1964)].

[7]J. J. Vuillemin and M. G. Priestly, Phys. Rev. Letters 14, 307 (1965); J. J. Vuillemin, Phys. Rev. 144, 396 (1966).

[8]A. J. Freeman, J. O. Dimmock, and A. M. Furdyna, J. Appl. Phys. 37, 1256 (1966); see also O. K. Andersen, thesis, Technical University of Denmark, 1969 (unpublished); Ref. 18 below.

[9]We use the scheme of J. C. Slater [Phys. Rev. 51, 846 (1937)] as programmed by Dr. J. H. Wood, to whom we are grateful.

[10]H. Montgomery (unpublished); R. Doclo, S. Foner, and A. Narath, J. Appl. Phys. 40, 1206 (1969).

[11]F. M. Mueller, Phys. Rev. 153, 659 (1967).

[12]B. C. Stoner, Proc. Roy. Soc. (London) A165, 372 (1938); E. P. Wohlfarth, Phys. Letters 3, 17 (1962).

[13]F. Herman and S. Skillman, *Atomic Structure Calculations* (Prentice-Hall, Englewood Cliffs, N. J., 1963).

[14]R. E. Watson and A. J. Freeman (unpublished).

[15]A. Y. C. Yu and W. E. Spicer, Phys. Rev. 169, 497 (1968).

[16]D. E. Eastman, J. Appl. Phys. 40, 1387 (1969).

[17]L. R. Windmiller and J. B. Ketterson, Phys. Rev. Letters 21, 1076 (1968).

[18]O. K. Andersen and A. R. Mackintosh, Solid State Commun. 6, 285 (1968); also private communication.

[19]T. L. Loucks, *Augmented Plane Wave Method* (Benjamin, New York, 1967).

[20]A. J. Freeman and D. D. Koelling, Bull. Am. Phys. Soc. 14, 28 (1969).

[21]E. C. Snow, J. T. Waber, and A. Switendick, J. Appl. Phys. 37, 1342 (1966).

[22]E. C. Snow, Phys. Rev. 171, 785 (1968); 172, 708 (1968).

[23]G. H. Wannier, Phys. Rev. 52, 191 (1937).
[24]L. P. Bouckaert, R. Smoluchowski, and E. Wigner, Phys. Rev. 50, 58 (1936).
[25]J. Friedel, P. Lenglart, and G. Leman, J. Phys. Chem. Solids 25, 781 (1964); P. Lenglart, G. Leman, and J. P. Lelieur, *ibid.* 27, 377 (1966); L. F. Mattheiss, Phys. Rev. 139, A1893 (1965).
[26]L. Hodges, H. Ehrenreich, and N. D. Lang, Phys. Rev. 152, 505 (1966).
[27]D. Liberman, J. T. Waber, and D. T. Cromer, Phys. Rev. 137, A27 (1965).
[28]G. Weisz, Phys. Rev. 149, 504 (1966).
[29]J. C. Slater, Phys. Rev. 81, 385 (1951).
[30]L. J. Sham and W. Kohn, Phys. Rev. 145, 561 (1966).
[31]V. Heine, Phys. Rev. 153, 671 (1967).
[32]F. M. Mueller, J. B. Ketterson, and L. R. Windmiller, Phys. Rev. (to be published).
[33]F. M. Mueller, J. W. Garland, M. H. Cohen, and K. H. Bennemann (unpublished).
[34]G. Chouteau, R. Fourneaux, K. Gobrecht, and R. Tournier, Phys. Rev. Letters 20, 193 (1968), and references therein.
[35]G. Gladstone, M. A. Jensen, and J. R. Schrieffer, in *Superconductivity*, edited by R. D. Parks (Marcel-Dekker, New York, 1968).
[36]S. Foner and E. J. McNiff, Jr., Phys. Rev. Letters 19, 1438 (1967).
[37]L. R. Windmiller, J. B. Ketterson, and S. Hornfeldt, J. Appl. Phys. 40, 1291 (1969).
[38]L. R. Windmiller, J. B. Ketterson, and S. Hornfeldt, Phys. Rev. Letters (to be published).
[39]D. D. Koelling, A. J. Freeman, and F. M. Mueller, J. Appl. Phys. (to be published).

PHYSICAL REVIEW B VOLUME 1, NUMBER 12 15 JUNE 1970

Grüneisen Parameters of Cubic Metals

P. K. Sharma and Narain Singh
Physics Department, University of Allahabad, Allahabad, India
(Received 15 January 1970)

The Grüneisen parameters of alkali metals, noble metals, and aluminum have been calculated at different temperatures from available pressure derivatives of elastic constants, using the Chéveau model for their lattice dynamics. The calculation is carried out by a modified Houston's method. The calculated Grüneisen parameters show reasonably satisfactory agreement with experimental measurements.

I. INTRODUCTION

The lattice dynamics of metals has been the subject of considerable theoretical and experimental literature. Early theoretical workers completely neglected the influence of conduction electrons. In the past few years, several models[1-3] have been worked out for studying the lattice vibrations in metals by introducing the influence of conduction electrons in Born–Von Kármán theory. Many of them, however, do not satisfy the periodic symmetry properties of the lattice. Lax[4] has attributed this inadequacy to the neglect of translational invariance of the lattice. Recently, Krebs[5] has propounded a model by incorporating the suggestion of Lax which meets the symmetry requirements of the lattice. However, this model suffers from a serious drawback of internal equilibrium. The derivative of long-range screened Coulomb interaction energy does not vanish in the equilibrium configuration. Quite recently, Chéveau[6] has proposed a simple model for the lattice dynamics of cubic metals which satisfies the symmetry properties and preserves internal equilibrium without recourse to any external force. In this model, the ion-ion interaction is described by the first two terms in the Taylor expansion of the potential energy, as in the model of Bhatia.[2] The electronic contribution is, however, calculated from linearized Thomas-Fermi theory for the whole crystal.

In the present paper, we have utilized the Chéveau model to calculate the Grüneisen parameters of alkali metals, noble metals, and aluminum at different temperatures. The stimulus for this study was dictated by the recent appearance of thermal expansion and pressure derivative of elastic constants for these metals.[7,8]

II. THEORY

The temperature variation of the thermal expansion is most conveniently represented by the dimensionless Grüneisen parameter $\gamma(T)$, defined by

$$\gamma(T)=\beta V B_T/C_v \ , \qquad (1)$$

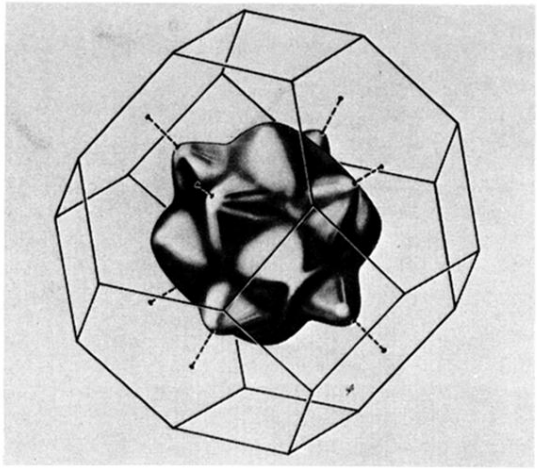

FERMI ELECTRON SURFACE FOR PALLADIUM

FIG. 3. Γ-centered sixth-band electron sheet of palladium. Although topologically equivalent to a sphere, this sector of the Fermi surface shows large distortions. As is discussed in the text, the sheet is primarily *d* like rather than plane-wave-like.

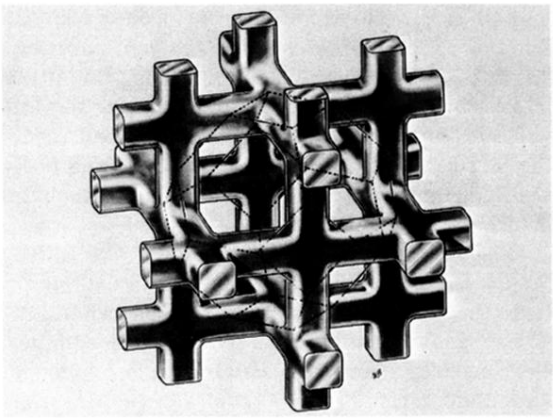

FERMI HOLE SURFACE FOR PALLADIUM

FIG. 4. *X*-centered hole sheet of palladium. This sheet is formed from the fifth-band electrons and forms an open network in the extended zone. As is discussed in the text, this sheet is primarily *d*-like.